10-28-2008

Composition Control and Localization of S^{2-} in CdSSe Quantum Dots Grown FROM $Li_4[Cd_{10}Se_4(SPh)_{16}]$

Ryan Oyler
Florida State University

Recommended Citation

Oyler, Ryan, "Composition Control and Localization of S^{2-} in CdSSe Quantum Dots Grown FROM $Li_4[Cd_{10}Se_4(SPh)_{16}]$" (2008). *Electronic Theses, Treatises and Dissertations.* Paper 2437.

FLORIDA STATE UNIVERSITY

COLLEGE OF ARTS AND SCIENCES

COMPOSITION CONTROL AND LOCALIZATION OF S^{2-} IN CdSSe QUANTUM DOTS GROWN FROM $Li_4[Cd_{10}Se_4(SPh)_{16}]$

By

RYAN EDWARD OYLER

A Thesis submitted to the
Department of Chemistry and Biochemistry
in partial fulfillment of the
requirements for the degree of
Masters of Science

Degree Awarded:
Fall Semester, 2008

The members of the Committee approve the Thesis of Ryan Oyler defended on October 28, 2008.

Geoffrey F. Strouse
Professor Directing Thesis

Sanford A. Safron
Committee Member

Oliver Steinbock
Committee Member

Approved:

Joseph B. Schlenoff, Chair, Department of Chemistry and Biochemistry

The Office of Graduate Studies has verified and approved the above named committee members.

ACKNOWLEDGEMENTS

I would like to acknowledge the superior help of Derek Lovingood in the gathering and interperting of the experimental data presented in this thesis. Financial support of the project was provided through the National Institute of Health (NBIB 7 R01 EB000832) and the National Science Foundation (DMR-0701462). The TEM images were measured at the National High Magnetic Field Laboratory at Florida State University (NSF DMR-9625692) with the assistance of Dr. Yan Xin. The solid state NMR measurements were performed at the Florida State University Chemistry Deparment NMR facility with the assistance of Dr. Randall Achey.

TABLE OF CONTENTS

List of Figures v
List of Equations vi
List of Abbreviations vii
Abstract viii

1. INTRODUCTION TO SEMICONDUCTOR NANOCRYSTALS 1

    1.1 Introduction to Semiconductors 1
    1.2 Nanocrystal Semiconductors (Quantum Dots) 4

2. COMPOSITION CONTROL AND LOCALIZATION OF S^{2-} IN CdSSe QUANTUM DOTS GROWN FROM $Li_4[Cd_{10}Se_4(SPh)_{16}]$ 8

    2.1 Abstract 8
    2.2 Experimental Methods 10
        2.2.1 Chemicals 10
        2.2.2 Instumentation 10
        2.2.3 Synthesis of CdSSe QDs from $Li_4[Cd_{10}Se_4(SPh)_{16}]$ 12
        2.2.4 Synthesis of CdSe QDs from $Li_4[Cd_{10}Se_4(SePh)_{16}]$ 12
        2.2.5 Homogeneous Acid Etching of CdSSe QDs 12
    2.3 Results and Discussion 14
        2.3.1 Cluster Grown Nanocrystals 14
        2.3.2 Elemental Distribution in the As-Prepared CdSSe 15
        2.3.3 Nature of the CdSSe Alloy 19
        2.3.4 Qualitative Model of the QD 21
        2.3.5 Conclusion 23

APPENDIX A 25

APPENDIX B 27

REFERENCES 29

LIST OF FIGURES

Figure 1.1 Electronic Band Structure of Bulk CdSe and CdS 2

Figure 1.2 Semiconductor Energy Band Gap Plots 3

Figure 1.3 Confinement Effects of CdSe and CdS 5

Figure 1.4 Doping Effects on Energy Band Gap 6

Figure 2.1 Possible Composition Scenarios..14

Figure 2.2 TEM Images, Abosportption Plots, and XRD Plots of CdSSe Nanocrystals......15

Figure 2.3 ^{13}C CPMAS NMR of CdSSe Nanocrystals...17

Figure 2.4 Ligand Ratio versus Size Plot of CdSSe Nanocrystals 18

Figure 2.5 Absorption versus Size Plot of CdSSe Nanocrystals 20

Figure 2.6 [S^{2-}] Percentage of Anions versus Size and Etching 22

Figure 2.7 Models of CdSSe Nanocrystals Composition 23

LIST OF EQUATIONS

Equation 1.1 Effective Mass Equation..5

Equation 2.1 Debye-Scherrer Formula 11

Equation 2.2 Concentration-Dependent Effective Mass Equation 20

LIST OF ABBREVIATIONS

CP-MAS – Coupled Proton Magic Angle Spinning
HDA – Hexadecylamine
NMR – Nuclear Magnetic Resonance
pXRD – Powder X-ray Diffraction
QD – Quantum Dot
SAED – Selected Area Electron Diffraction
SPh – Thiophenol
TEM – Transmission Electron Microscopy
TGA – Thermogravimetric Analysis
TOPO – Trioctylphosphine Oxide
XRF – X-ray Fluorescence

ABSTRACT

Reproduced with permission from Journal of the American Chemical Society, submitted for publication. Unpublished work copyright 2008 American Chemical Society.

The development of ternary nanoscale materials with controlled cross-sectional doping is an important step in the use of chemically prepared quantum dots for nanoscale engineering applications. We report cross-sectional, elemental doping for the formation of an alloyed CdSSe nanocrystal. The nanocrystal is prepared from the thermal decomposition of $Li_4[Cd_{10}Se_4(SPh)_{16}]$. The sulfur incorporation arises from a surface mediated degradation of a $[Cd(SPh)_4]^{2-}$ tetrahedral passivant tightly bound to the growing quantum dot surface. In the alloy, we identify a pure CdSe nucleus of ~ 1.5 nm consistent with the predictions of nucleation theory. As the particle grows, S^{2-} incorporation increases until ~3.5 nm, at which point an equilibrium of the S^{2-}/Se^{2-} incorporation rate is attained. The use of molecular clusters to allow controlled defect ion incorporation can open new pathways to more complex nanomaterials.

CHAPTER 1

INTRODUCTION TO SEMICONDUCTOR NANOCRYSTALS

Section 1.1: Introduction to Semiconductors[1]

Semiconductors are comprised of solid materials with periodic atomic structures, lattices, and exhibit conductivities between that of metals and insulators. They are identified by the unique property of energy band gaps. It is this property that directly defines the electronic response of a semiconductor to thermal and electromagnetic stimuli and the effects of elemental impurities.

A crystal lattice is constructed by repeating patterns of atom arrangements. Lattices are categorized by the characteristic lengths and angles of their unit cell. A unit cell is a smaller volume representative of the lattice containing a basic arrangement of atoms which are regularly repeated throughout the lattice. The unit cell parameters (lengths and angles) of a semiconductor define the energy levels populated by electrons in the ground state and those available for conduction. Energy band gaps are essentially a consequence of atoms in a lattice with their structural properties defined by the geometry and elemental concentration of the lattice.

The important electronic difference between periodic solids and isolated atoms is the hybridization of atomic wave functions throughout the lattice and the resulting redistribution of electrons. In ionic bonding insulators, the valence electrons are held tightly to atoms (localized) and the electrically charged atoms are bonded by coulombic forces. These tightly held electrons are not available for conduction and give the material its defining electrically insulating characteristic. Metals are typified by delocalization of electrons across the lattice which facilitates conduction. Like ionic bonded solids metals are heavily influenced by coulombic forces of positively and negatively charged particles. However in the case of a metal, the negative charge is not bound tightly to the atomic lattice but exists freely distributed throughout the solid susceptible to electric fields. Semiconductors are crystalline materials where the availability of electrons for conduction can vary over a relatively large range.

In insulators and semiconductors the conduction band, empty states available for electron promotion, and the valence band, filled states occupied by ground state electrons, are separated in energy by unavailable or forbidden states. The forbidden states exist in energy from the highest energy of the valence band to the lowest energy of the conduction band and are collectively known as the energy band gap.

The energy band structure is unique for all solids. The relative configuration of valence band, conduction band, and band gap is a product of the lattice created by equilibrium of the interatomic forces. The discrete states of isolated metal atoms form into solids where the conduction and valence bands overlap or are partially filled. Electrons and available unoccupied states necessary for conductions exist at nearly the same energy in metals and allow for their high electrical conductivity.

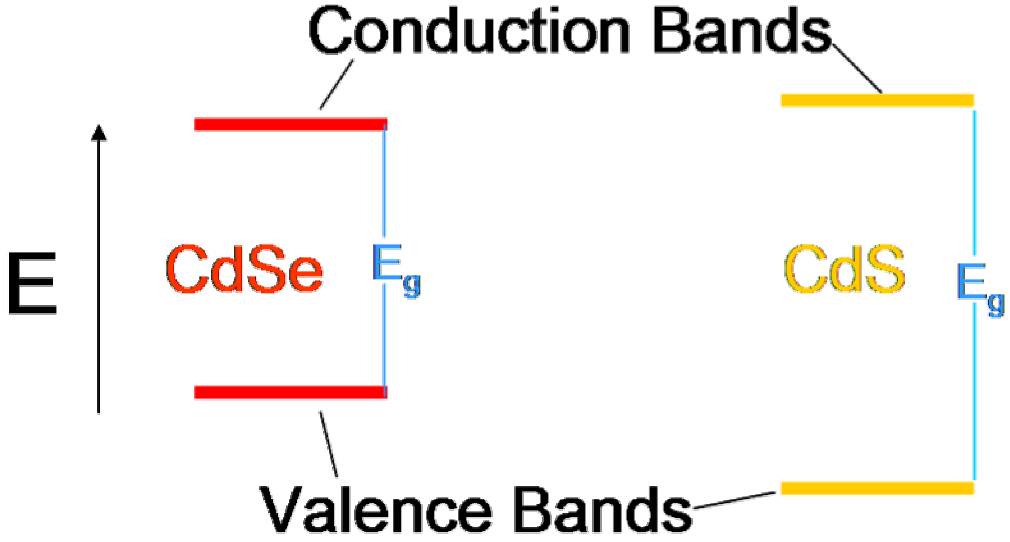

Figure 1.1 Relative energy band structures of bulk CdSe and CdS.

Both insulators and semiconductors have band gaps. The essential difference is the magnitude; insulators have large band gaps while semiconductors have relatively small band gaps. Without thermal or optical stimulation insulators and semiconductors do not have electrons and available unoccupied states nearby in energy. Thermal energy induced in a semiconductor at room temperature can excite a reasonable amount of electrons into the conduction band, while room temperature will not affect an insulator with a band gap an order of magnitude greater. The thermal and optical increase in the mixing of electrons and available unoccupied states leads to a relatively large increase in conductivity and is the defining property of semiconductors. The band gap energies (E_g) of two semiconductors of interest in this thesis are CdSe and CdS, which are 1.73 eV and 2.42 eV respectively.

The energy band structure of these semiconductors can be represented as featureless bars with an arbitrary *x*-axis as shown in Figure 1.1. More information can be attained and used to predict properties of semiconductors by plotting the energy state of electrons against their propagation constant or wave vector, **k**, which directly relates to the momentum of an electron.

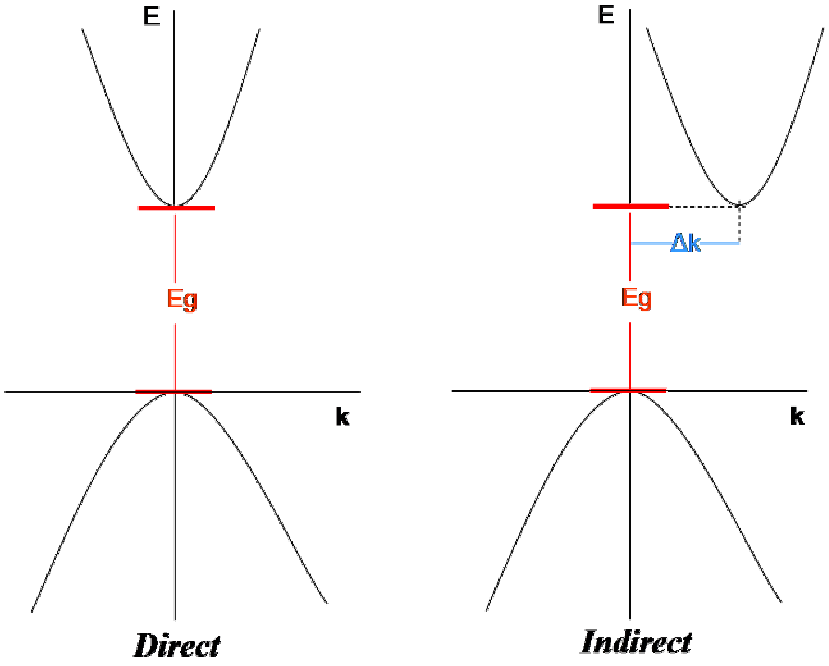

Figure 1.2 Energy versus propagation constant plot of near band gap states for direct and indirect semiconductors.

The resulting plot **k** vs. *E* of the electrons shows a complex relationship of the energy bands. The band gap is not uniform over all momentum states, experiencing maxima and minima in the valence and conduction bands (Figure 1.2). When a minimum in the conduction band and maximum in the valence band of a semiconductor have the same **k** value it is known as a direct semiconductor. When the **k** values of those extrema are not equal the semiconductor is indirect and the energy transition of excited electrons returning to the ground state requires a change in momentum. Direct semiconductors are generally chosen for devices that require efficient light emission. Both CdSe and CdS are direct semiconductors.

Effective mass is useful concept for understanding the electronic properties of semiconductors. Electrons traveling in a solid are not completely freed from the crystal lattice as an electron in a vacuum would be. To account for the interaction of electrons (and holes) with the potential energy environment of the atomic lattice the particles can be treated with equations designed for free electrons by modifying their mass value. Computing the properties of particles is this manner is known as an effective mass calculation. The effective mass considers the average **k** value in three dimensional space of an electron occupying a particular energy band. The calculation of hole and electron effective masses in a semiconductor is a very complex process and yields unique values for each band and sub-band. In Chapter 2 the effective mass approximation is used to investigate the electronic properties of CdSe and CdSe materials using semi-empirical values for effective masses to calculate band gap energies.

Section 1.2: Nanocrystal Semiconductors (Quantum Dots)

Bulk semiconductors display a continuum of states known as energy bands, as described in the previous section. When the spatial dimensions of a semiconductor material shrink to the order of nanometers these continuum of states dissolves into a set of allowed, discrete states. At the nanoscale, materials have reached a size at which the three-dimensional volume of their lattice has started to confine the wave function of the electrons and affects the energy levels available for electron occupation. The band gap energy of semiconductors increases from the bulk value as it reaches the size of a nanocrystal. This confinement effect is directly observable as a size-dependency of the absorption spectra in semiconductor nanocrystals.

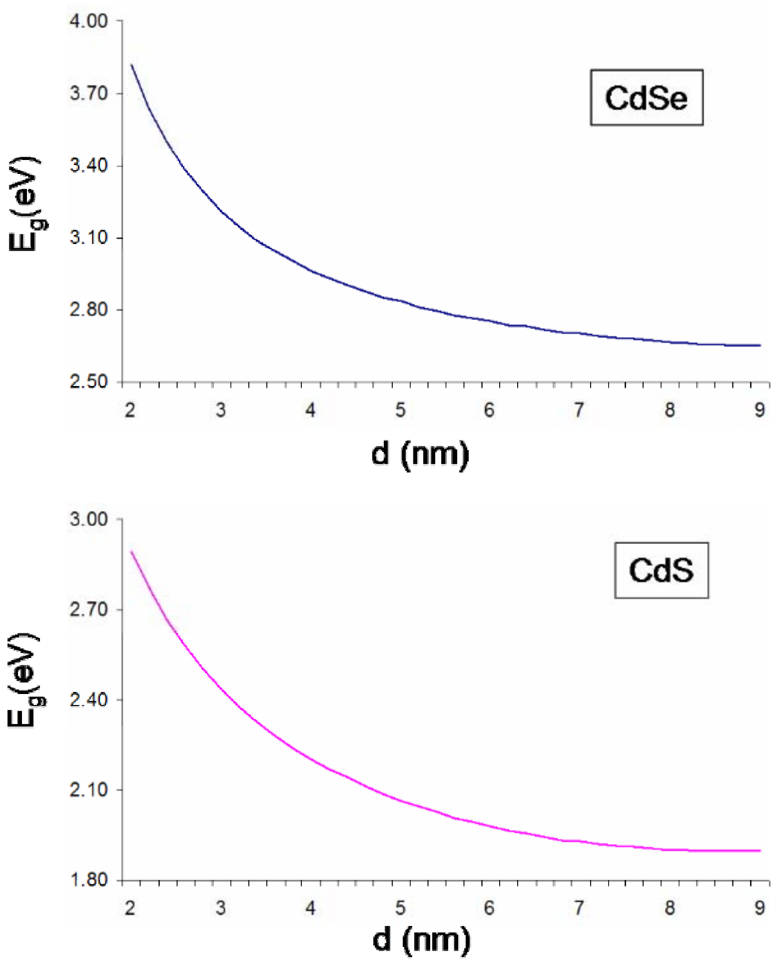

Figure 1.3 Confinement effects of E_g , band gap energy, vs. d, diameter of the nanocrystal, for pure CdSe and CdS nanocrystals

The plots in Figure 1.3 show the effective mass approximations of the band gap energy versus diameter for spherical CdSe and CdS nanocrystals. Smaller semiconductor nanocrystal ave wider energy bad gaps and therefore increased absorption energies.

Size-dependent effective mass approximations[2] add appropriate quantum mechanical terms for the quantization of the bands into discrete energy levels. The second order size dependent term accounts for the confinement of the available states in a potential well. The first order term is negative to account for the coulombic attraction of the electron-hole pair in a reduced volume. The details of the potential are hidden within the effective masses generated for the electron and hole of a material, and as such are only as accurate as the calculated masses.

$$E = E_g^{bulk} + \frac{h^2}{8r^2}\left(\frac{1}{m_e m_0} + \frac{1}{m_h m_0}\right) - \frac{1.8\, e^2}{4\pi\varepsilon\varepsilon_0 r} - \frac{0.124\ e^4}{h^2 (2\varepsilon\varepsilon_0)^2}\left(\frac{1}{m_e m_0} + \frac{1}{m_h m_0}\right)^{-1} \qquad \textbf{(Eq. 1.1)}$$

By generating good fits for band gap energy vs. size data the average effective mass of a material can be solved for as first and second order parameters.[3] Effective mass constants calculated in this manner for pure semiconductors can be used to predict the shift in band gap energy as the average elemental concentration of a material changes. In statistical doping of semiconductors this has a dramatic effect on electronic band structure and defines the range of band gap energies available to a semiconductor at nanocrystal size regimes.

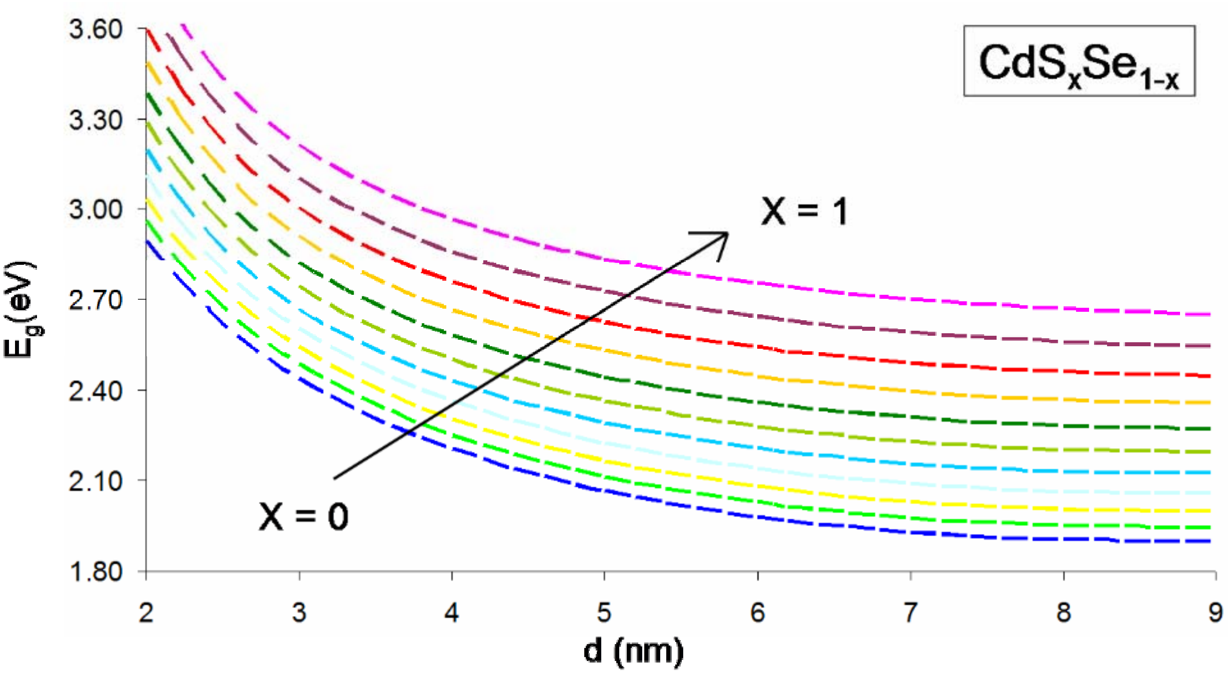

Figure 1.4 Confinement effects for CdS_xSe_{1-x} alloys. The colors indicate band gap energy shift as anion concentration changes from pure CdSe (x=0) to pure CdS (x=1).

The combination of CdS and CdSe in a semiconductor nanocrystal can have a variety of effects depending on the distribution of the anions across the nanocrystal. So called 'core-shell' effects arise when the concentration of S^{2-} or Se^{2-} is completely segregated and the volume of one is completely encompassed by the other. In a nanocrystal where the core is a CdSe lattice and the surround material is CdS (a CdSe/CdS core-shell) the band gap of CdS contains the CdSe band gap within its energy range. In other words, the lowest available conduction band state of CdS is a *higher* energy state than CdSe's analogous state and the highest occupied valence band state of CdS is of *lower* energy than CdSe's analogous state. This type of core-shell nanocrystal (Type I) localizes excitons generated in the CdSe core, increasing the probability of electron-hole recombination and the quantum yield of photoluminescence. The inverse distribution, a CdS/CdSe core-shell Type II, the conduction band of the CdSe lies at a lower potential energy than the CdS allowing the excited electron to easily delocalize to the shell of the semiconductor. CdSe/CdS have found application in light emission studies while the CdS/CdSe nanocrystal has potential value in photovoltaic experiments.

If the concentration of anions in a CdS_xSe_{1-x} nanocrystal is evenly distributed in stoichiometric ratios the band gap energy will shift proportionally. The absorption wavelength values of alloyed ternary nanocrystals do fall between the pure binary values, and experimental, as well as theoretical, values for CdS_xSe_{1-x} compounds have been shown to follow a progression that mirrors that of the bulk alloys.[3] The shift in elemental concentration is an important factor used to calculate band gap energy of a semiconductor but does not appear to have a size-dependent component.

CHAPTER 2

COMPOSITION CONTROL AND LOCALIZATION OF S^{2-} IN CdSSe QUANTUM DOTS GROWN FROM $Li_4[Cd_{10}Se_4(SPh)_{16}]$

Section 2.1: Introduction

Preparation of emissive quantum dots (QDs) have evolved to the point where very narrow size dispersions of the desired binary or ternary semiconductor can be prepared routinely, whether through the use of molecular reactants,[1-3] single source dual component precursors,[4] or single source inorganic clusters.[5-8] The growth of the II-VI QDs from the inorganic cluster, while well documented,[11-27] is mechanistically poorly understood. Depending on the reaction temperature and conditions, we[8] and others[10] have observed variable concentration of S^{2-} incorporation into CdSe QDs grown from $[Cd_{10}Se_4(SPh)_{16}]^{4-}$, the parentage of which can be traced to phenylthiolate decomposition at the QD surface.

S^{2-} incorporation is not surprising based on the earlier studies of Wang and Herron on CdS formation from the cluster $[Cd_{10}Se_4(SPh)_{16}]^{4-}$. In this study they observed a surface mediated cleavage reaction between two bridging SPh^- groups with ensuing production of S^{2-} and loss of diphenyl sulfide.[28] In the solid solution the anion distribution throughout the QD may exist as a homogeneous, heterogeneous, gradient, or perhaps a core-shell[3,29] depending on the competition between phenylthiolate decomposition, phenylthiolate concentration, and rate of S^{2-} versus Se^{2-} addition to a growing QD surface. The possibility of a core-shell motif was first suggested by Gamelin et al[10] due to the observation of enriched S^{2-} content at the QD surface; however, a core-shell motif is not necessary to observe enrichment of S^{2-} at the surface based on our NMR observation[30] of strongly bound SPh^- at the QD surface, which would result in the identical conclusion of S^{2-} enrichment but not imply a core-shell motif. The remarkable stability of the phenylthiolate at the surface (impervious to ligand exchange in pyridine) and the lack of detrimental effects on the quantum yield implies that the phenylthiolate anion exists as the $[Cd(SPh)_4]^{2-}$ tetrahedral capping motif on these cluster grown QD materials, as suggested in our earlier study.[30] These results have prompted a more in-depth study into understanding the quality of the resultant QD grown from the inorganic cluster source, the nature of the anion distribution in the solid solution, and the complexity associated with the incorporation of defect ions into a growing QD.

By correlating X-ray fluorescence (XRF), thermogravimetric analysis (TGA), NMR, and UV-Vis absorption, we demonstrate the formation of a CdSSe gradient as the QD grows, with enrichment of S^{2-} in the alloy. The optical absorption of the CdSe materials shows a blue shift in the energy due to the increasing S^{2-} content, as predicted by the effective mass approximation for a ternary semiconductor. The S^{2-} concentration is higher in XRF than estimated by absorption. The aberrant S^{2-} content measured by micro-analytical techniques represents a combination of the S^{2-} alloy enrichment as the particle grows plus the presence of the Cd-phenylthiolate species, while the absorption only reflects the band gap tuning by alloy formation. The surface of the alloy is passivated by a combination of TOPO and the tetrahedral phenylthiolate species $[Cd(SPh)_4]^{2-}$ over all sizes in the study. TGA confirms that the SPh^- groups are in the form of $[Cd(SPh)_4]^{2-}$, and are not lost upon thermal cycling, but rather collapse into an alloyed structure analogous to the findings of Wang and Herron and suggested by Gamelin. NMR correlated to XRF and effective mass approximation studies lead us to conclude that a S^{2-}/Se^{2-} ion distribution approaching 66% at the surface exists for QDs that are > 3.5 nm in size, while for a 1.5 nm QD a pure CdSe with phenylthiolate surface capping exists. The increasing S^{2-} content in the alloy for QDs above 3.5 nm correlates with the thermal activation of the surface mediated Cd-phenylthiolate decomposition process.

Section 2.2: Experimental Methods

Section 2.2.1: Chemicals

The molecular clusters $Li_4[Cd_{10}Se_4(SPh)_{16}]$ and $Li_4[Cd_{10}Se_4(SePh)_{16}]$ were prepared as previously described.[31-33] Hexadecylamine (HDA, 90%), 85% H_3PO_4, 12 M HCl, were used without further purification.

Section 2.2.2: Instrumentation

Elemental composition for Cd^{2+}, S^{2-}, and Se^{2-} was carried out in an Oxford Instruments ED2000 X-ray fluorescence (XRF) spectrometer with a Cu-K_α source. The mole ratio for Cd^{2+} to Se^{2-} to S^{2-} for each sample was analyzed using XRF with four repeat analyses for statistical validation. For a standard XRF measurement, the powdered samples were completely dissolved in 90% HNO_3 to allow total elemental composition to be analyzed. In order to allow compatibility with the XRF sample holder, the samples were heated to remove excess NO_x and then diluted to ~5 mL with a 2% HNO_3 solution. All measurements were carried out at the K_α line for the element, Cd^{2+} (23.1 keV), Se^{2-} (11.2 keV), and S^{2-} (2.3 keV). Total counts need to be above 10 cps to reduce error in the analysis. Calibration curves were generated using commercially prepared 1000 ppm elemental standards in 2% HNO_3, which results in accuracies of ±3 ppm for Cd^{2+}, ±4 ppm for Se^{2-}, and ±16 ppm for S^{2-}. Composition analysis of bulk samples was used to further validate the method.

Optical absorption was analyzed in a 1-cm cell in toluene ($\sim 1 \times 10^6$ mol) using a Cary 50 UV-Vis spectrophotometer. Powder X-ray diffraction (pXRD) was carried out on a Rigaku MAX 300 Ultima 3 diffractometer using Cu-K_α ($\lambda = 1.5418$ A) with the d-spacing calibrated to a Si^0 standard to verify crystal motif. Using the Debye-Scherrer formula (Eq. 2.1) the QD diameter was calculated,

$$\tau = \frac{K\lambda}{\beta \cos\theta}$$

(Eq. 2.1)

where τ is the QD diameter, λ is the X-ray wavelength, β is the full width at half maximum of the peak, θ is the angle at the peak, and K is the shape factor. The <110> peak was used to calculate the QD diameter to eliminate complications from overlapping reflections. QD sizes and morphology were verified and the shape factor calibrated by transmission electron microscope (TEM) for select samples using a JEOL-2010 operated at 200 kV. Selected area electron diffraction (SAED) built into the TEM system was used to investigate the crystalline structures of the particles. The QDs were dispersed on holey carbon (400 mesh) from a toluene solution.

Thermogravimetric Analysis (TGA) samples were placed into alumina crucibles for analysis on an SDT 2960 (Simultaneous DSC TGA) and were heated to 300 °C or 500 °C at a rate of 2 °C/min under a flow of N_2 gas at 60 mL/min. Percent weight loss was determined for each sample using the accompanying TA Universal Analysis 2000 software package. A 4.0 and 5.7 nm CdSSe alloy grown from the cluster were measured by TGA at 300 °C and at 500 °C and the resultant powder analyzed by XRF for S^{2-}, Se^{2-}, and Cd^{2+} content.

Solid State ^{13}C CP-MAS NMR experiments were performed at room temperature on a Varian Unity/Inova 500 MHz spectrometer with a 2.5-mm broadband MAS probe double tuned to ^{1}H (500.3 MHz) and the X channel to ^{13}C (125.8) MHz. A spinning speed of 12 kHz was used on all experiments. ^{13}C CP-MAS experiments were performed on $Li_4[Cd_{10}Se_4(SPh)_{16}]$ and TOPO capped CdSSe grown from $Li_4[Cd_{10}Se_4(SPh)_{16}]$. ^{13}C CP-MAS experiments were acquired using an acquisition time of 50 ms, a recycling delay of 3 sec, a contact time of 1.6 ms and a ^{1}H 90^{o} pulse length of 5 μs. The chemical shifts were referenced to TMS (0 ppm).

Section 2.2.3: Synthesis of CdSSe QDs from $Li_4[Cd_{10}Se_4(SPh)_{16}]$

A series of CdSSe QDs (2 – 5 nm) were prepared from the single source inorganic cluster $Li_4[Cd_{10}Se_4(SPh)_{16}]$ in HDA at 230 °C. QDs below 1.8 nm were also prepared and isolated by carrying out the identical reaction at lower temperature (120 °C). The generic reaction was carried out in a flame dried round bottom flask in which 200 g of hexadecylamine (HDA) was added, degassed, and placed under Ar at 70 °C for ~1.5 h; and then raised to 120 °C. To the HDA was added 2.0 g of $Li_4[Cd_{10}Se_4(SPh)_{16}]$ as a powder, and the reaction temperature was increased to 230 °C at an approximate rate of 1-2 °C /min. Five large aliquots (15 mL) were isolated every 10-20 nm. These samples were isolated from the reaction mixture and purified using standard dissolution - precipitation protocols, in which the aliquots were solvated in toluene (~5 mL), methanol (~5 - 10 mL) was added to induce precipitation, the sample was centrifuged and the precipitate collected (3x). A final purification step was applied by dissolving the precipitate (20 mg) into liquid TOPO (1 g, 80 °C) for 5 min and precipitation of the QD from the TOPO using the above dissolution-precipitation procedure above. The samples were stored under vacuum following isolation of the solid.

Section 2.2.4: Synthesis of CdSe QDs from $Li_4[Cd_{10}Se_4(SePh)_{16}]$[33]

A pure CdSe QD was grown from the molecular precursor $Li_4[Cd_{10}Se_4(SePh)_{16}]$ in an analogous fashion to the alloyed materials. Briefly, to a flame dried round bottom flask 40 g of HDA was added, degassed, and placed under Ar at 70 °C for ~1.5 h. To the HDA was added 400 mg of pure Se^{2-} cluster, $Li_4[Cd_{10}Se_4(SePh)_{16}]$, prepared by previously published methods.[33] The reaction was heated to 230 °C and monitored by absorption spectra until the desired sizes were reached. This sample was cleaned by selective precipitation with toluene/methanol, followed by TOPO exchange.

Section 2.2.5: Homogeneous Acid Etching of CdSSe QDs.[34]

Uniform etching of the crystallite faces can be accomplished with a II-VI specific etchant using a 1:1 (V:V) 12 M HCl:85% H_3PO_4 . To etch the QD samples, the acid etchant (50-200 µL depending on degree of etching desired) was added to 50 mg of the CdSSe QD in excess TOPO with 5 mL of toluene and allowed to stir for ~1 min. The solution was quenched and the etched QDs precipitated by addition of methanol. The size of the QD was verified by TEM and absorption analysis.

Section 2.3: Results and Discussion

Section 2.3.1: Cluster Grown Nanocrystals

QD growth, whether from elemental or single source precursors is controlled by the nucleation and growth steps of the reaction. Growth begins with a pure nucleus (nucleation step) and can incorporate defects as the crystallite grows depending on the concentrations and the kinetics for the specific ion addition to the growing nanocrystal surface.[35] When the single source cluster reaction is carried out in a strongly coordinating solvent, it is presumed that QDs are generated from a similar mechanism as proposed by Wang and Herron for formation of CdS bulk materials from $[Cd_{10}S_4(SPh)_{16}]^{4-}$.[28,36] The mechanism involves cluster coupling induced by loss of the terminal phenylthiolate, with subsequent growth by a combination of cluster rearrangement into the bulk structure and S^{2-} incorporation by decomposition of the $[Cd(SPh)_4]^{2-}$ tetrahedral caps. The decomposition can be mechanistically described as a simple Lewis acid catalyzed nucleophilic aromatic substitution to produce diphenyl sulfide and S^{2-}.[37,38] The ratio of S^{2-} incorporation from the capping moieties is controlled by the reaction temperature and conditions. In a strongly passivating solvent, QDs can be formed instead of bulk materials due to kinetic trapping by ligand passivation.[5]

For nanocrystals grown from $[Cd_{10}Se_4(SPh)_{16}]^{4-}$, the probability of S^{2-} incorporating into the growing nanocrystal with subsequent alloy formation therefore would not be surprising. The temperature of the reaction will dictate the percentage of phenylthiolate decomposition and subsequent S^{2-} content in the growing QD. The nature of the alloy that could be formed by this reaction process can be described as several simplistic models, namely a homogeneous solid-solution (uniform or a gradient from core to surface),[3] a heterogeneous solid-solution,[3,39] or core-shell.[10,40] (Figure 2.1).

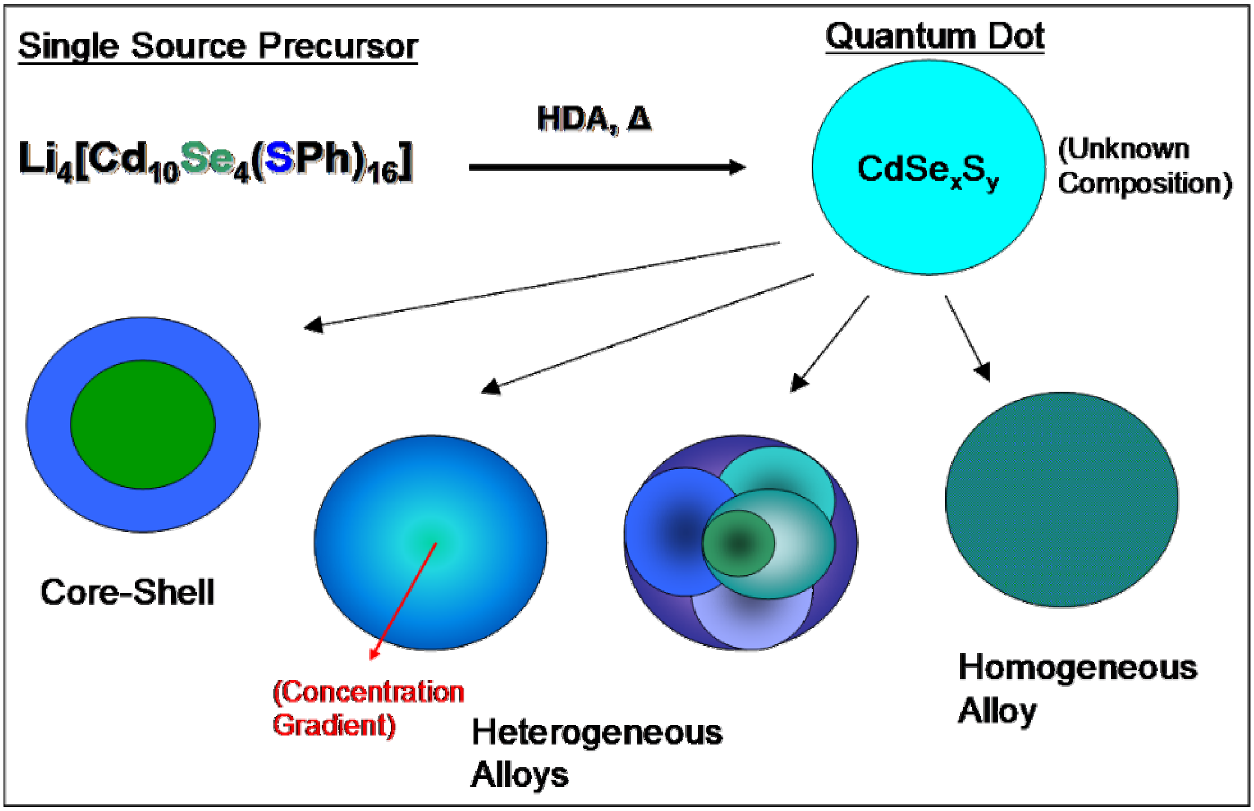

Figure 2.1 Possible composition scenarios for a CdSSe QD grown from the cluster, $Li_4[Cd_{10}Se_4(SPh)_{16}]$.

Highly faceted, narrow size disparity CdSSe nanocrystals (± < 7% for 5.7 nm sample) were isolated from the single source cluster route in the size range from 1.6 – 5.7 nm, as measured by TEM, absorption, and pXRD (Figure 2.2). pXRD (Figure 2.2D), as well as TEM FFT analysis indicate the CdSe and CdSSe QDs have wurtzite symmetry, while the CdS QDs are cubic. Control samples of pure CdSe and CdS were also isolated from single source clusters using the respective pure chalcogenide.

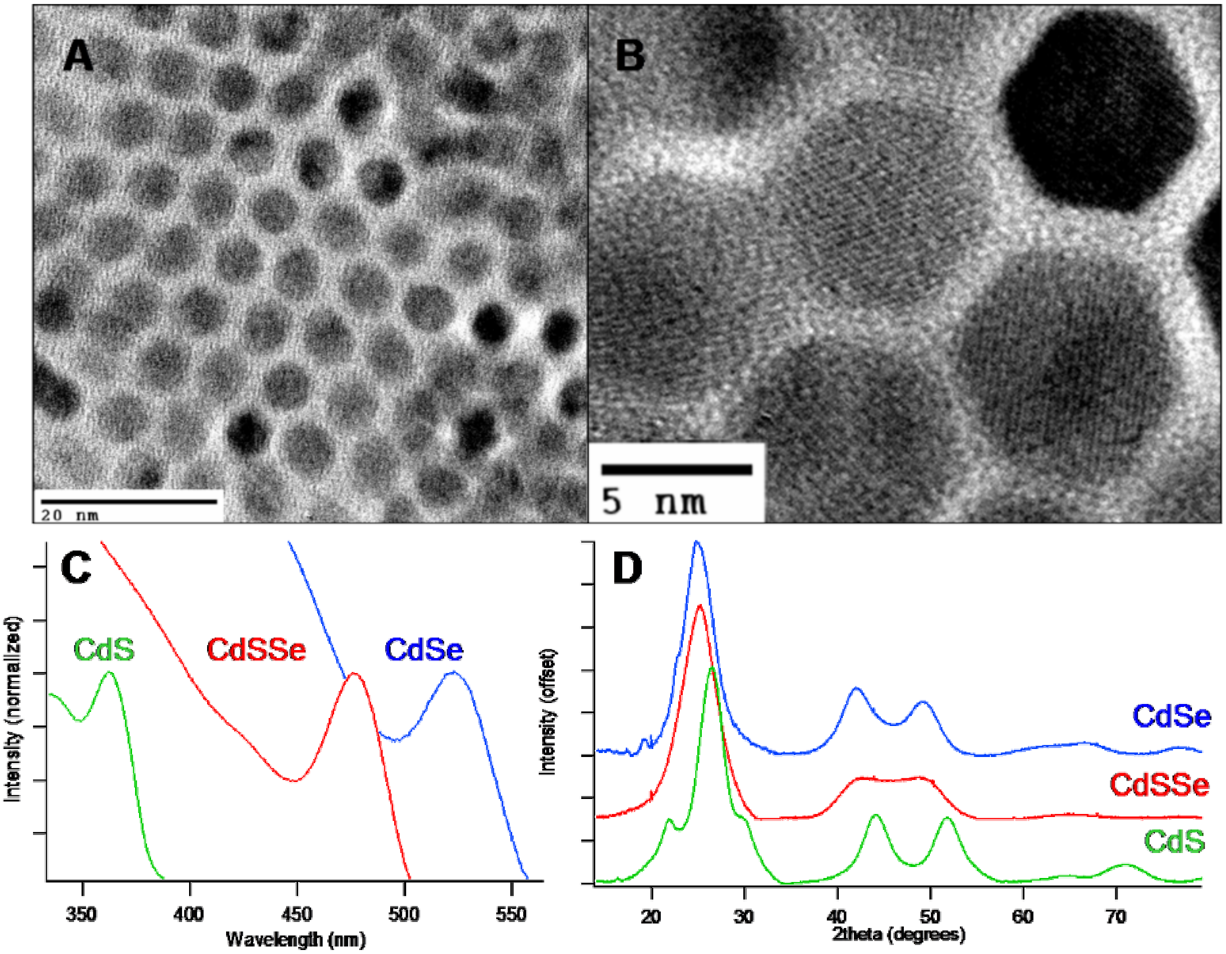

Figure 2.2 A) TEM image of dispersed CdSSe QDs. 5.7 nm QDs with total S2-:Se2- is 66:34 by XRF. **B)** HRTEM images of the same sample with visible lattice fringes. **C)** Absorption spectra of near same size (~2.4 nm from pXRD Scherrer-Debye analysis) CdSe, CdSSe, and CdS QDs. CdSSe QD S2-:Se2- is 36:64 by XRF. **D)** pXRD spectra of ~2.4 nm QD samples.

Section 2.3.2: Elemental Distribution in the As-Prepared CdSSe

In Table 2.1, the Se^{2-} concentration found for the series of isolated CdSSe QDs grown from the single source cluster $Li_4[Cd_{10}Se_4(SPh)_{16}]$ measured by XRF on samples completely digested in HNO_3 is shown (Supplemental Figure A.1). Inspection of Table 2.1 indicates an increase in S^{2-} content as the QDs increase in size up to ~3.5 nm, where the S^{2-}/Se^{2-} ratio asymptotes at ~66% sulfur. At 1.55 nm the S^{2-} content approaches 0% suggestive of pure nuclei formation in this reaction. In all reactions a high concentration of S^{2-} is observed, although for reaction temperatures of 120 °C, the S^{2-} content appears to be lower, either due to size or S^{2-} availability in the reaction mixture. It is worth noting that the XRF cannot distinguish between

S^{2-} and SPh^- contributions to the S^{2-}/Se^{2-} ratio in the QD and therefore cannot distinguish between S^{2-} ions alloyed into the QD or bound in a core-shell motif. Although many micro-analytical techniques can be used to evaluate S^{2-} content, XRF is the most accurate for analyzing the S^{2-} to Se^{2-} ratios, as there are no complications from overlapping peaks as observed in XPS.[41,42]

	XRF % [Se]*	Eff. Mass Appox. % [Se]**	Abs. λ (nm)	XRD (Scherrer) diameter (nm)
CdSSe (230 °C)	64	78	477	2.44
	77	81	511	3.03
	67	77	517	3.16
	58	77	522	3.26
	69	76	502	2.93
	58	89	457	1.96
	75	90	489	2.32
	85	87	498	2.56
	66	76	507	2.97
	60	74	516	3.26
	37	78	560	4.42
	36	78	567	4.71
	52	70	473	2.57
	60	77	488	2.64
	61	71	497	2.96
	58	78	509	2.97
	55	77	514	3.10
	36	78	539	3.65
	35	81	548	3.81
	36	82	564	4.30
	39	73	567	5.13 [5.09]
	34	69	570	5.74 [5.78]
CdSSe (120 °C)	74	84	486	2.40
	76	79	466	2.25
	77	81	450	2.05
	88	99	430	1.56
CdSe	100	-	532	2.77
	100	-	526	2.65
	100	-	519	2.46
	100	-	498	2.22
CdS	0	-	352	2.41

Table 2.1 Experimental results for S^{2-}/Se^{2-} composition, QD diameter by Scherrer broadening of <110> pXRD reflection, and exciton absorption ($1s_e$ -$1s_h$). ***** is the Se^{2-} concentration of total S^{2-} and Se^{2-} concentration measured by XRF while ****** is the Se^{2-} concentration affecting the electronic structure. Bracketed numbers are diameters verified by HRTEM. Highlighted samples are depicted in

To rationalize the S^{2-} content, the presence or absence of phenylthiolates at the QD surface must first be analyzed. The presence of phenylthiolate bound to a QD surface either as a terminal group or as a tetrahedral capping group in the form $[Cd(SPh)_4]^{2-}$ will substantially modify the actual S^{2-} content measured in a QD sample resulting in a significant skewing of the XRF results, and thus the conclusion of the material motif. The CdSSe samples in this study were analyzed by solid state ^{13}C CP-MAS. These samples were subjected to TOPO exchange at 80 °C for 5 min and re-isolated from the TOPO solution using standard re-precipitation techniques prior to the NMR analysis.

In the NMR data we observed the presence of SPh^- on all sample sizes in remarkably high ratios confirming the presence of phenylthiolate at the surface and more importantly the inability to remove the phenylthiolate by standard ligand exchange protocols. The NMR data for a 3.2 nm CdSSe sample ^{13}C spectra is shown in Figure 2.3 for the aromatic region and the complete NMR spectra is in the Supplemental Figures (Supplemental Figure A.2). The aromatic resonances arising from SPh^- can be clearly observed in the spectra. The resonances can be assigned to the phenylthiolate carbons at 132.16 ppm (ortho), 127.51 ppm (meta), and 123.03 ppm (para) with no observable alpha carbon. The NMR frequencies are consistent with the values measured in $Li_4[Cd_{10}Se_4(SPh)_{16}]$ at 137.49 ppm (alpha), 134.57 ppm (ortho), 127.17 ppm (meta), and 123.32 ppm (para), as well as out earlier report on 2 nm CdSe.[30]

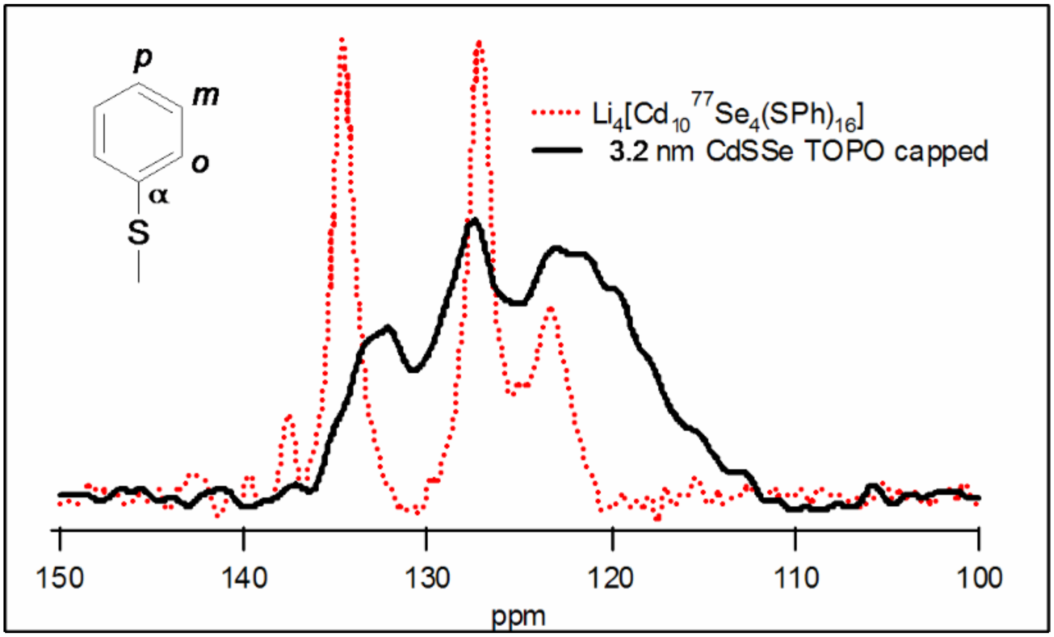

Figure 2.3 ^{13}C CP-MAS NMR of the cluster and a nanocrystal grown from the cluster. The aromatic region is shown with overlapping signals of phenylthiolate ligands.

The representative NMR data shows conclusively that SPh$^-$ is present in these materials. However, it is important to note that the S^{2-} content reported in Table 2.1 is too high to be accounted for by merely the presence of SPh$^-$ at the surface, particularly at the largest sizes where ~70% S^{2-} content is measured by XRF. Although a core-shell motif could help explain this observation, our ^{13}C NMR studies clearly demonstrate Se^{2-} at the surface in the ^{1}H-^{77}Se CPMAS experiments.[30] To properly project the CdSSe composition and thus the elemental distribution, the quantity and characteristics of SPh$^-$ at the QD surface must be better understood.

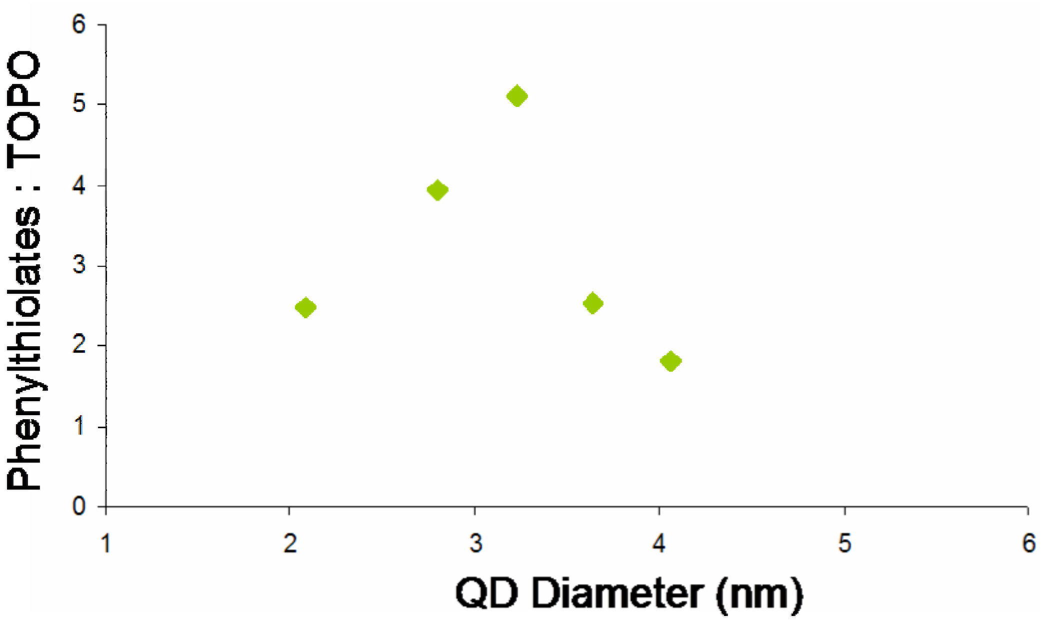

Figure 2.4 CdSSe QD samples plotted as function of diameter versus phenylthiolate to TOPO ligand ration measured by ^{13}C MAS NMR.

A semi-quantitative measure of the phenylthiolate ligation can be extracted by integration of the ^{13}C CP-MAS NMR signals for phenylthiolate and TOPO (Figure 2.4). A plot of the phenylthiolate content versus size is intriguing, as it suggests the SPh$^-$ content increase with increasing size up to at least 3 nm, and than decreases as the QD grows. Ligand exchange by TOPO, pyridine or HDA does not modify the observed phenylthiolate concentration ratio in these materials. This observation is consistent with our earlier publication[30] where the phenylthiolate was observed to be remarkable robust on the QD surface, exhibiting a lack of exchange by pyridine at 70 °C or TOPO at 80 °C. Consistent with this observation TGA on a 3.5 nm CdSSe and 5.7 nm CdSSe exhibit marked differences for S^{2-} loss following heating to 600 °C. The mass loss at temperatures up to 600 °C most likely arises from the thermal degradation of two SPh^- ligands with production of a free S^{2-} and diphenylsulfide, as observed in the earlier TGA studies by Wang and Herron. The smaller QD shows significant loss of S^{2-} following heating to 600 °C (42% → 21%), while the 5.7 nm QD shows insignificant changes in S^{2-} (66% → 63%). The lower loss for S^{2-} corroborates the lower SPh^- composition on the QD surfaces analyzed by the NMR data.

The nature of the phenylthiolate capping found by solid state NMR on CdSSe suggests the SPh^- exists as the tetrahedral capping group ($[Cd(SPh)_4]^{2-}$) due to the difficulty of ligand exchanging the phenylthiolate group and the remarkably high percentage of SPh^- compared to TOPO seen in these materials. The binding of $[Cd(SPh)_4]^{2-}$ instead of SPh^- would account for the inability to readily exchange the phenylthiolate for another passivant and the observed high ratio of S^{2-} to Se^{2-} observed in the XRF micro-analytical data for the QDs.

Section 2.3.3: Nature of the CdSSe Alloy

While the presence of SPh^- on the QD surface rules out a simple core-shell motif to explain the S^{2-} enrichment, it does not rule out S^{2-} ion incorporation into the growing QD. The actual nature of the alloy is still unknown, whether a homogeneous or inhomogeneous alloy (Figure 2.1) is formed during the reaction. Insight into the nature of the alloy is readily gained by considering the impact of formation of a solid solution on the electronic properties of the semiconductor QD using an effective mass approximation to account for the tuning of the semiconductor band gap by the alloying of the ternary ion. The change in the exciton absorption as a function of size and composition can be generated by use of the theoretical model described by Rosenthal et al[3] for CdSSe QD homogeneous alloys. By applying the size dependent confinement formula of the effective mass expression (Eq. 2.2) and utilizing known energy shifts for pure cluster grown samples,[43] an expression can be generated for the shift in the exciton as a function of elemental composition,

$$E_g(x,d) = x\left[E_g(\mathrm{CdS},\infty) + \frac{a_1}{d} + \frac{c_1}{d^2}\right] + (1-x)\left[E_g(\mathrm{CdSe},\infty) + \frac{a_2}{d} + \frac{c_2}{d^2}\right] - b(d)x(1-x) \qquad \textbf{(Eq. 2.2)}$$

where *a* and *c* represent the reduced mass of the e^- and h^+, but are fit as empirical parameters in this case, *d* is the QD diameter, and *b* is the bowing constant describing the nonlinear effects of ion doping.

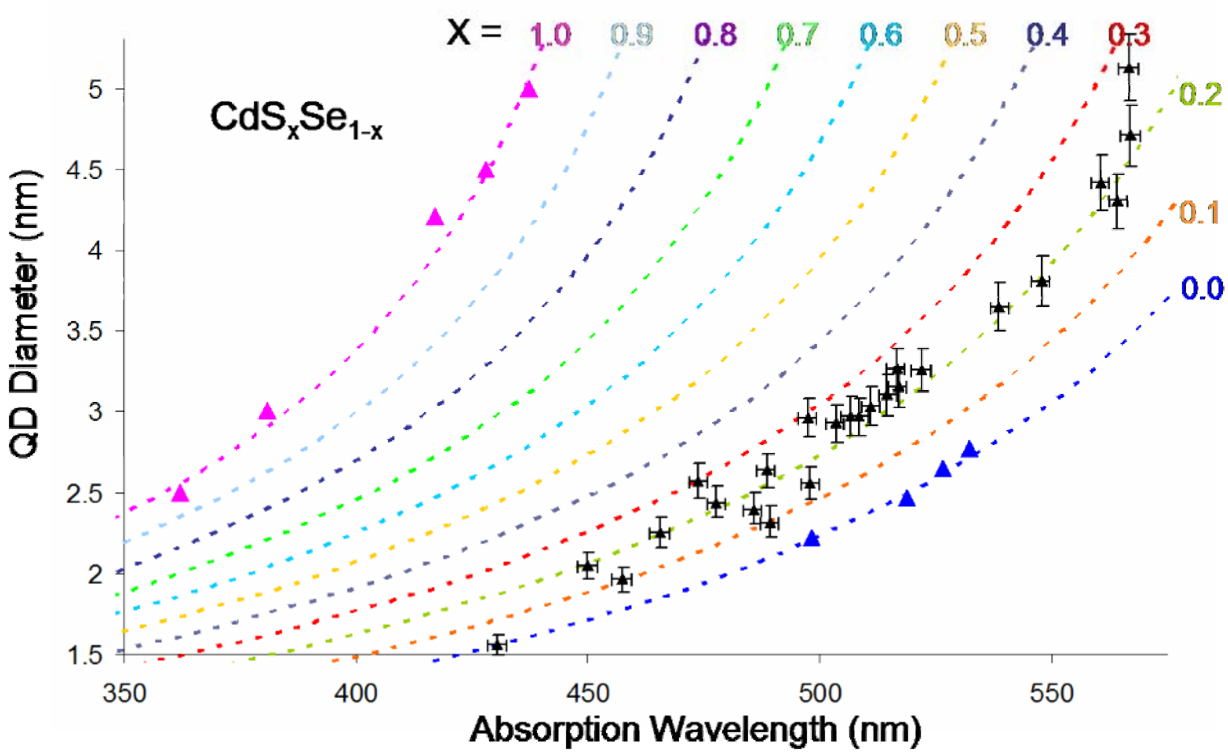

Figure 2.5 CdSSe QD samples (black triangles) grown from $Li_4[Cd_{10}Se_4(SPh)_{16}]$. Sizes measured by pXRD Scherrer-Debye analysis and calibrated by HRTEM. Dashed lines are theoretical effective mass plots for the indicated concentrations of S^{2-}:Se^{2-}. Blue triangles are pure CdSe QD samples. Magenta triangles are pure CdS QD samples from Ref. 43.

Figure 2.5 shows the change in the energy for the first exciton absorption for the series of CdS_xSe_{1-x} QDs in this study overlaid with theoretical plot of the effective mass approximation. Inspection of the absorption value for the exciton versus the measured size shows there is a shift in the energy gap when compared to pure CdSe or CdS QDs of the same size. The first excitonic transition exhibits a blue-shift of 41 nm for a QD of the same size. The core-shell motif, where CdSe and CdS phases are completely segregated, does induce a shift in the absorption edge, but has a much weaker (~8 times less) effect at low dopant concentrations.[3,40] The observed shift in the first exciton transition of CdSSe relative to CdS and CdSe QDs provides direct and conclusive evidence of S^{2-} incorporation into the lattice. Although the effective mass equation is an approximation for describing the QD absorption properties, the experimental plots support a homogeneous alloy formation. The details of the alloy whether uniform or a gradient from core to surface is not defined by the absorption data alone, and only the correlation of all the experiments can provide a map of the formed alloy.

Section 2.3.4: Qualitative Model of the QD

If we assume the growth of a QD follows crystallization theory, with a pure nuclei forming first and the QD growth governed by thermodynamic equilibrium for S^{2-} and Se^{2-} addition to the growing material,[35] we predict for a hetero-nuclear reaction, a pure nucleus is formed from the binary components prior to the formation of the ternary alloy. For cluster reactions, the incorporation of S^{2-} to form an alloy will be dominated by the temperature of the reaction, since the decomposition mechanism is temperature dependent; and the concentration of surface bound Cd-phenylthiolate, since the rate of atom addition is dictated by the microscopic reactivity of the QD surface.

Thermodynamics predict that the activity of adding ions will have inherently different rates for ion incorporation.[2,44] Therefore, for QD growth from the cluster, $[Cd_{10}Se_4(SPh)_{16}]^{4-}$, we expect a pure CdSe nuclei (nucleation), followed by increasing S^{2-} to Se^{2-} ratios as the particle grows due to Se^{2-} depletion and increasing Cd-phenylthiolate decomposition as the reaction progresses with reaction temperature (Ostwald ripening). As the reaction progresses, a constant value for the S^{2-} to Se^{2-} ratio will occur when the rate of S^{2-} and Se^{2-} incorporation comes to equilibrium.

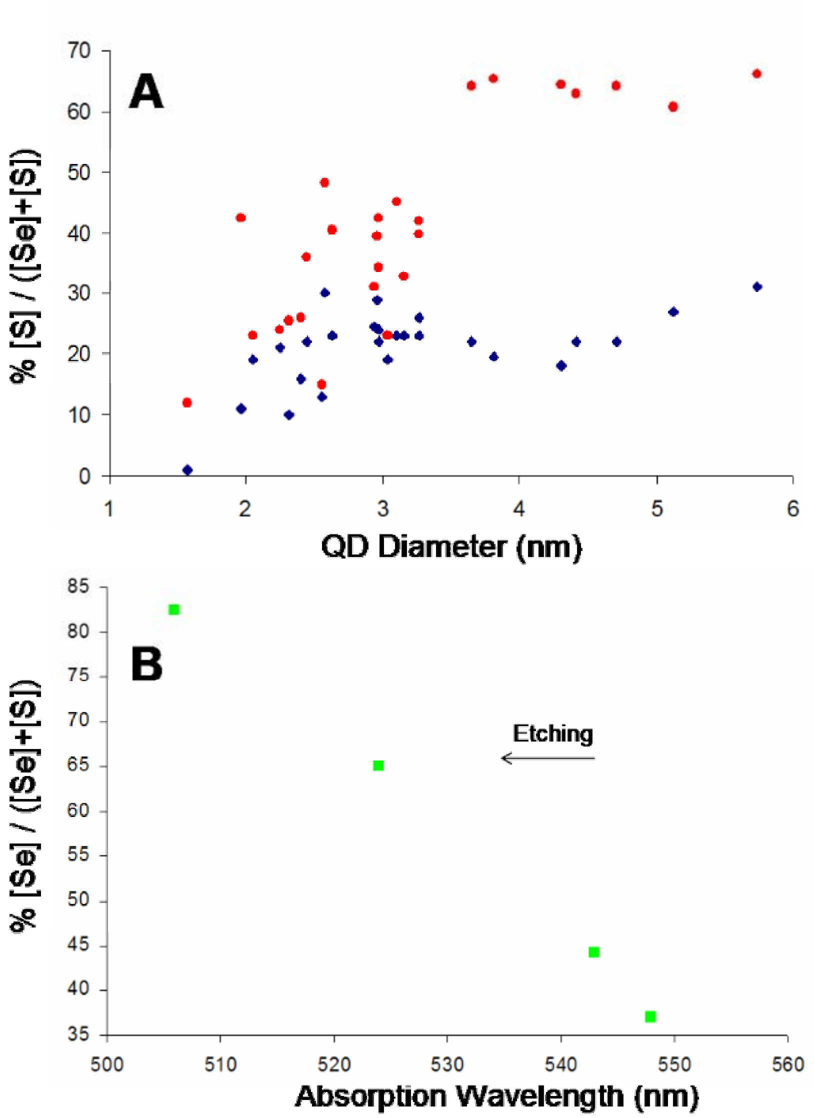

Figure 2.6 A) CdSSe QD samples plotted as function of diameter versus %[Se^{2-}] measured by XRF (red circles) and by effective mass approximation (blue diamonds). **B)** Etched CdSSe QD sample plotted as the absorption wavelength of the first exciton vs. %[Se^{2-}] by XRF.

A plot of the S^{2-} percentage versus size extracted from XRF and absorption data is shown in Figure 2.6A. An increase in S^{2-} content is observed from a value of 1% (12% XRF) at 1.5 nm to a constant value of 25% (66% XRF) above 3.5 nm based on Eq. 2. The experimental data is consistent with the proposed growth mechanism. The nucleation step is evidenced by the nearly pure composition for a 1.5 nm QD observed in Figure 2.6A. Efforts by Gamelin et al have pointed towards the critical nuclei for CdSe to be roughly 1-2 nm in size, in agreement with our observation.[35] As the particle grows, the S^{2-} concentration increases linearly up to 3.5 nm and asymptotes at a steady state concentration as predicted by the crystallization process.

While the results of the study are consistent for either XRF or absorption analysis, the latter probes lattice composition whilst the former reports both lattice and surface ligand contributions. The mismatch of the two values observed in Figure 2.6A above 3.5 nm is assigned to the formation of a S^{2-} enriched surface, which necessarily includes the Cd-phenylthiolate moiety. The high S^{2-} content in the XRF data is clearly associated with a surface S^{2-} enrichment, when the S^{2-}/Se^{2-} ratio is mapped for the etching of a 5.1 nm QD with HCl/ H_3PO_4 (Figure 2.6B). A linear reduction in S^{2-} content is observed for the first 1 nm of etching of the QD. This allows a final model to be proposed for these materials that bridge the earlier observation by Gamelin and our observation of phenylthiolate at the surface of QDs grown by the cluster approach.

Section 2.3.5: Conclusion

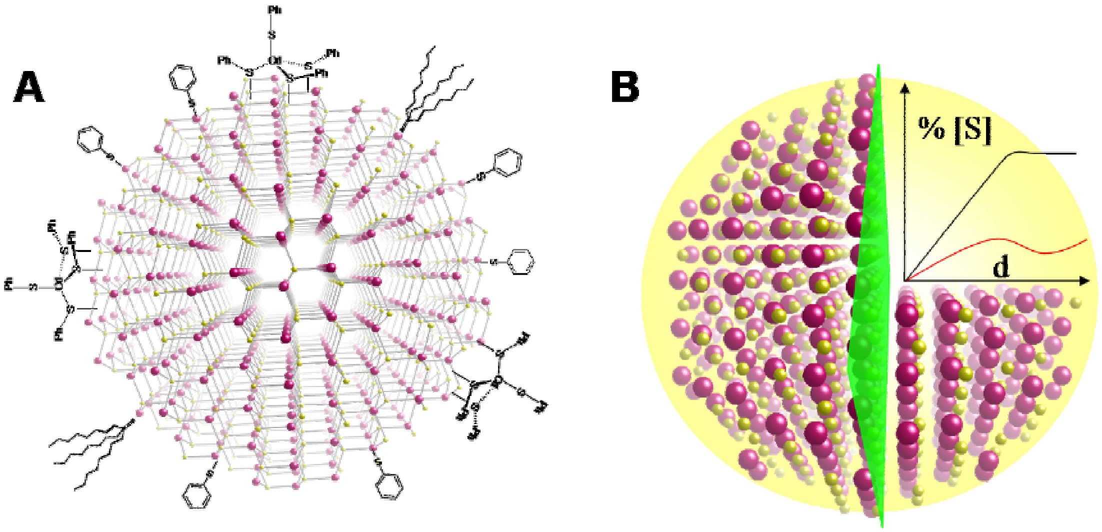

Figure 2.7 Models of CdSSe QD. **A)** Crystal structure of a CdSSe QD with organic ligands passivating the surface viewed normal to the <110> plane. **B)** CdSSe QD cross-section cut on the <110> and <002> (green) planes. Plot depicts the percent [S^{2-}] of total anions as the CdSSe QD's diameter increases during growth from a pure CdSe core to a CdSSe alloy. Average trendline for the XRF measurements (black) and effective mass approximation (red) are pictured.

In Figure 2.7, the model for S^{2-} distribution throughout the QD is proposed. At the core, a pure CdSe nuclei of ~1.5 nm exists. As the particle continues to grow, phenylthiolate decomposition increases the S^{2-} content in the reaction and an alloy is formed. With increasing temperature the S^{2-} to Se^{2-} ratio varies in a gradient fashion from the center. The surface of the QD for materials below 3.5 nm is dominated by the appendage of $[Cd(SPh)_4]^{2-}$, which retards growth and provides a source for S^{2-} addition once thermal decomposition begins. Above 3.5 nm, the S^{2-} to Se^{2-} addition reaches equilibrium and a constant ratio of S^{2-} to Se^{2-} is observed. The contribution of phenylthiolate to the total S^{2-} content reduces substantially above this point as evidenced by the NMR data, and therefore has a smaller impact on the error from micro-analytical techniques.

The data supports a model where the Se^{2-} is not restricted to the core and the S^{2-} to the surface, as expected for a core-shell, but rather represents a solid solution whose composition is controlled by thermodynamic parameters, namely S^{2-} concentration, energetics of S^{2-} versus Se^{2-} addition to a growing QD, and the conversion from a kinetically controlled reaction to a thermodynamically equilibrated process. It is not surprising that the compositional distribution of the S^{2-} in the CdSSe QDs is quite complex if one considers the implications of nucleation theory and the influence of the precursor concentrations on the kinetics as the reaction progresses since the available reactant concentrations (S^{2-} vs. Se^{2-} vs. Cd^{2+}) are in constant flux.

APPENDIX A

SUPPLEMENTAL FIGURES

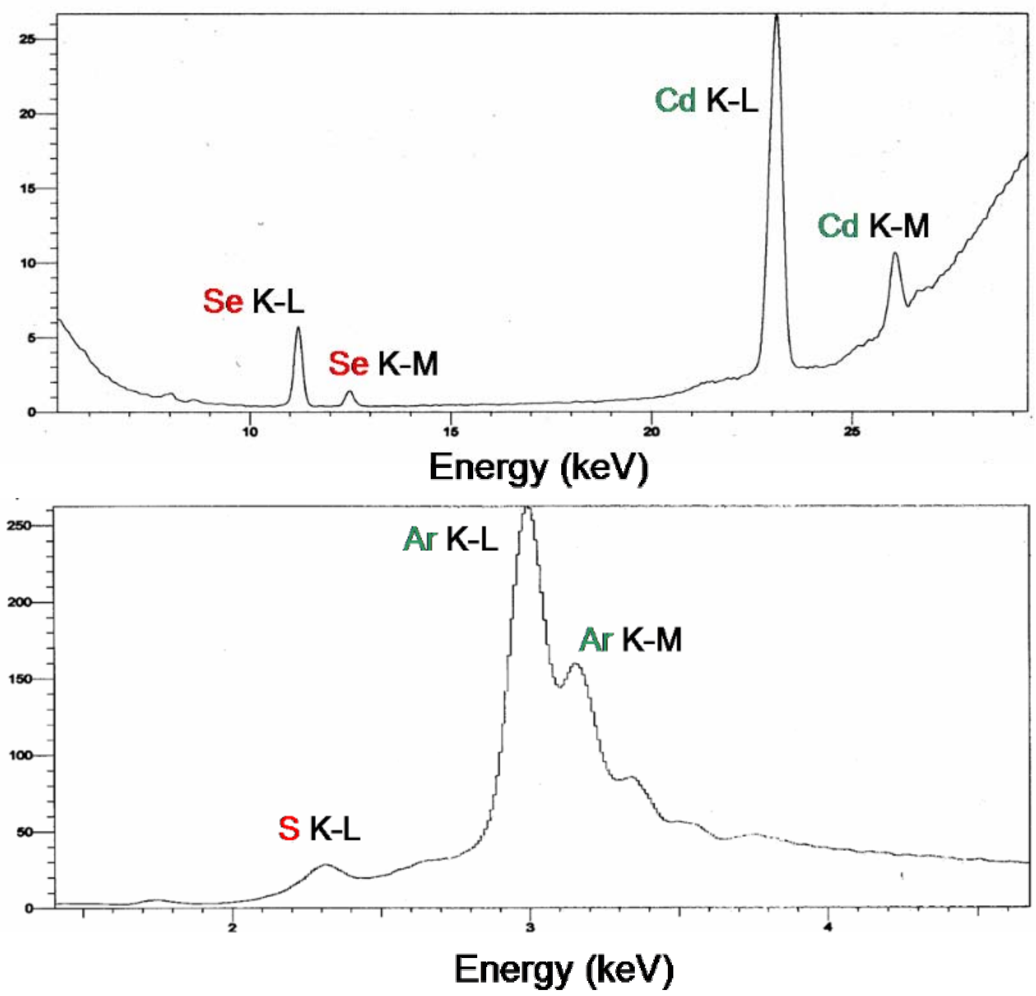

Supplemental Figure A.1 Sample XRF Spectra for CdSSe nanocrystals.

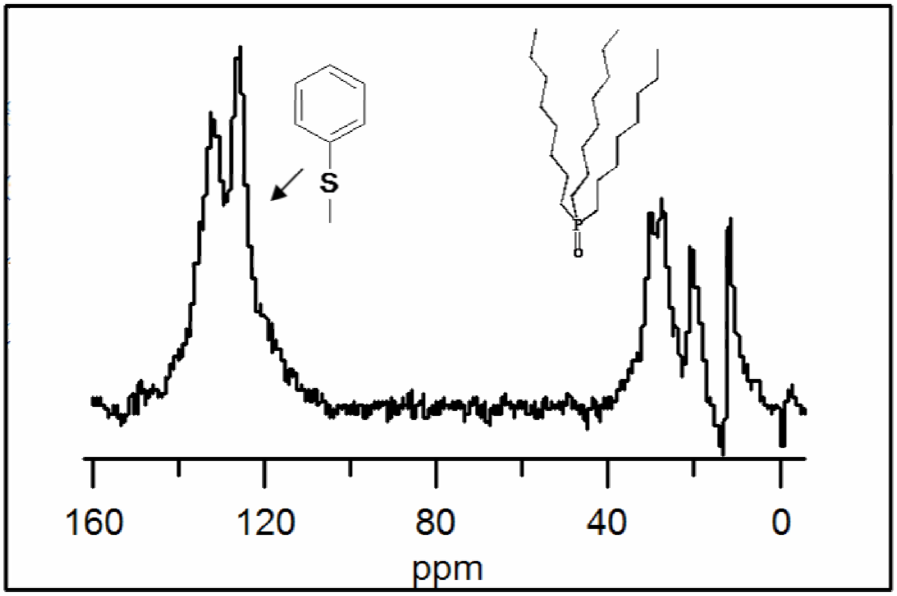

Supplemental Figure A.2 ^{13}C MAS NMR spectra of a 3.64 nm CdSSe QD after TOPO exchange.

APPENDIX B

ACS COPYRIGHT PERMISSION

American Chemical Society's Policy on Theses and Dissertations

Thank you for your request for permission to include **your** paper(s) or portions of text from **your** paper(s) in your thesis. Permission is now automatically granted; please pay special attention to the implications paragraph below. The Copyright Subcommittee of the Joint Board/Council Committees on Publications approved the following:

> Copyright permission for published and submitted material from theses and dissertations
> ACS extends blanket permission to students to include in their theses and dissertations their own articles, or portions thereof, that have been published in ACS journals or submitted to ACS journals for publication, provided that the ACS copyright credit line is noted on the appropriate page(s).
>
> Publishing implications of electronic publication of theses and dissertation material
> Students and their mentors should be aware that posting of theses and dissertation material on the Web prior to submission of material from that thesis or dissertation to an ACS journal may affect publication in that journal. Whether Web posting is considered prior publication may be evaluated on a case-by-case basis by the journal's editor. If an ACS journal editor considers Web posting to be "prior publication", the paper will not be accepted for publication in that journal. If you intend to submit your unpublished paper to ACS for publication, check with the appropriate editor prior to posting your manuscript electronically.

If your paper has **not** yet been published by ACS, we have no objection to your including the text or portions of the text in your thesis/dissertation in **print and microfilm formats**; please note, however, that electronic distribution or Web posting of the unpublished paper as part of your thesis in electronic formats might jeopardize publication of your paper by ACS. Please print the following credit line on the first page of your article: "Reproduced (or 'Reproduced in part') with permission from [JOURNAL NAME], in press (or 'submitted for publication'). Unpublished work copyright [CURRENT YEAR] American Chemical Society." Include appropriate information.

Submission to a Dissertation Distributor: If you plan to submit your thesis to UMI or to another dissertation distributor, you should not include the unpublished ACS paper in your thesis if the thesis will be disseminated electronically, until ACS has published your paper. After publication of the paper by ACS, you may release the entire thesis (**not the individual ACS article by itself**) for electronic dissemination through the distributor; ACS's copyright credit line should be printed on the first page of the ACS paper.

Use on an Intranet: The inclusion of your ACS unpublished or published manuscript is permitted in your thesis in print and microfilm formats. If ACS has published your paper you may include the manuscript in your thesis on an intranet that is not publicly available. Your ACS article cannot be posted electronically on a publicly available medium (i.e. one that is not password protected), such as but not limited to, electronic archives, Internet, library server, etc.

The only material from your paper that can be posted on a public electronic medium is the article abstract, figures, and tables, and you may link to the article’s DOI or post the article’s author-directed URL link provided by ACS. This paragraph does not pertain to the dissertation distributor paragraph above.

LIST OF REFERENCES

Chapter 1

(1) Streetman, B. G. *Solid State Electronic Devices (4th Ed.)* **1995**, Chapters 1-3, Englewood Cliffs, NJ: Prentice Hall, Inc.

(2) Brus, L. E. *J. Phys. Chem.* **1986**, *90*, 2555

(3) Swafford, L. A.; Weigand, L. A.; Bowers II, M. J.; McBride, J. R.; Rapaport, J. L.; Watt, T. L.; Dixit, S. K.; Feldman, L. C.; Rosenthal, S. J. *J. Am. Chem. Soc.* **2006**, *128*, 12299-12306.

Chapter 2

(1) Murray, C. B.; Noms, D. J.; Bawendi, M. G. *J. Am. Chem. Soc.* **1993**, *115,* 8706-8715.

(2) Peng Z. A.; Peng X. G. *J. Am. Chem. Soc.* **2001**, *123*, 1389-1395.

(3) Swafford, L. A.; Weigand, L. A.; Bowers II, M. J.; McBride, J. R.; Rapaport, J. L.; Watt, T. L.; Dixit, S. K.; Feldman, L. C.; Rosenthal, S. J. *J. Am. Chem. Soc.* **2006**, *128*, 12299-12306.

(4) Ludolph, B.; Malik, M. A.; O'Brien, P.; Revaprasadu, N. *Chem. Commun.* **1998**, 1849 – 1850.

(5) Cumberland, S. L.; Hanif, K. M.; Javier, A.; Khitrov, G. A.; Strouse, G. F.; Woessner, S. M.; Yun, C. S. *Chem. Mater.* **2002**, *14*, 1576-1584.

(6) Trindade, T.; O'Brien, P.; Zhang, X. M. *Chem. Mater.* **1997,** *9,* 523-530.

(7) Nair P. S.; Scholes G. D. *J. Mater. Chem.* **2006**, *16*, 467-473.

(8) Magana D.; Wei, X.; Strouse G. F.; *Phys. Rev. B.* **2008** 77, 115337.

(9) Archer, P. I.; Santangelo, S. A.; Gamelin, D. R. *Nano Lett.* **2007**, *7*, 1037-1043.

(10) Archer, P. I.; Santangelo, S. A.; Gamelin, D. R.; *J. Am. Chem. Soc*. **2007**, *129,* 9808-9818.

(11) Aslam, F.; Stevenson-Hill, J.; Binks, D. J.; Daniels, S.; Pickett, N. L.; O'Brien, P. *Chem. Phys.* **2007**, *334*, 45-52.

(12) Li, Y.; Feng, J.; Daniels, S.; Pickett, N. L.; O'Brien, P. *J. Nanosci. and Nanotech.* **2007**, *7*, 2301-2308.

(13) Magana, D.; Perera S. C.; Harter A. G.; Dalal N. S.; Strouse G. F. *J. Am.Chem. Soc.* **2006**, *128*, 2931-2939.

(14) Gerbec J. A.; Magana D.; Washington A.; Strouse G. F. *J. Amer. Chem. Soc.* **2005**, *127*, 15791-15800.

(15) Javier A.; Meulenberg R. W.; Yun C. S.; Strouse G. F.; *J. Phys. Chem. B* **2005**, *109*, 6999-7006.

(16) Meulenberg R.W.; Jennings T.; Strouse G. F. *Phys. Rev. B* **2004**, *70*, Art. No. 235311.

(17) Meulenberg R. W.; van Buuren T.; Hanif K. M.; Willey T. M.; Strouse G. F.; Terminello L. J. *Nano. Lett.* **2004**, *4*, 2277-2285.

(18) Javier A.; Strouse G. F. Chem. Phys. Lett. **2004**, *391*, 60-63.

(19) Berrettini M. G.; Braun G.; Hu J. G.; Strouse G. F. *J Amer. Chem. Soc.* **2004**, *126*, 7063-7070.

(20) Javier A.; Magana D.; Jennings T.; Strouse G. F. *Appl. Phys. Lett.* **2003**, *83*, 1423-1425.

(21) Aslam F.; Binks D. J.; Daniels S.; Pickett N.; O'Brien P. *Chem. Phys.* **2005**, *316*, 171-177.

(22) Aslam F.; Binks D. J.; Rahn M. D.; West D. P.; O'Brien P.; Pickett N; Daniels S. *J. Chem. Phys.* **2005**, *122*, Art. No. 184713.

(23) Aslam F., Binks D. J.; Rahn M. D.; West D. P.; O'Brien P.; Pickett N. *J. Mod. Opt.* **2005**, *52*, 945-953.

(24) Raola O. E.; Strouse G. F. *Nano. Lett.* **2002**, *2*, 1443-1447.

(25) Hanif K. M.; Meulenberg R. W.; Strouse G. F. *J. Amer. Chem. Soc.* **2002**, *124*, 11495-11502.

(26) Meulenberg R. W.; Strouse G. F. *Phys. Rev. B* **2002**, *66*, Art. No. 035317.

(27) Meulenberg R. W.; Bryan S.; Yun C. S.; Strouse G. F. *J. Phys. Chem. B* **2002**, *106*, 7774-7780.

(28) Farneth W. E.; Herron N.; Wang Y. *Chem. Mater.* **1992**, *4*, 916-922.
(29) van Embden, J.; Jasieniak, J.; Gomez, D. E.; Mulvaney, P. *Aust. J. Chem..* **2007**, *60*, 457-471.

(30) Berrettini M. G.; Braun G.; Hu J. G.; Strouse G. F. *J Amer. Chem. Soc.* **2004**, *126*, 7063-7070.

(31) Dance, I. G.; Choy, A.; Scudder, M. L. *J. Am. Chem Soc.* **1984**, *106*, 6285-6295.

(32) Choy, A.; Craig, D.; Dance, I. G.; Scudder, M. L. *J. Chem. Soc., Chem. Commun.* **1982**, 1246.

(33) Archer, P. I.; Santangelo, S. A.; Gamelin, D. R. *Nano Lett.* **2007**, *7*, 1037-1043.

(34) Wösten, W. J. *J. Appl. Phys*. **1962**, *33*, 246-247.

(35) Bryan, J. D.; Gamelin, D. R., In Karlin, K. D. *54*, *Progress in Inorganic Chemistry* **2005**, 47-126, Hoboken, NJ: John Wiley & Sons, Inc.

(36) Herron N.; Wang Y.; Eckert, H. *J. Am. Chem. Soc.* **1992**, *112*, 1322-1326.

(37) Nose, A.; Kudo, T. *Chem. Pharm. Bullet.* **1987**, *35*, 1770-6.

(38) Takagi, K. *Chem. Lett.* **1987**, *11*, 2221-4.

(39) Quarez E.; Hsu K. F.; Pcionek R.; Frangis N.; Polychroniadis E. K.; Kanatzidis M. G. *J. Am. Chem. Soc.* **2005**, *127*, 9177-9190.

(40) Peng, X. G.; Schlamp, M. C.; Kadavanich, A. V.; Alivisatos, A. P. *J. Am. Chem. Soc.* **1997**, *119,* 7019-7029.

(41) Bowen Katari, J. E.; Colvin, V. L.; Alivisatos, A. P. *J. Phys. Chem.* **1994***, 98,* 4109-4117.

(42) Bae W. K.; Char K.; Hur H.; Lee S. *Chem. Mater.* **2008,** *20,* 531–539.

(43) Khitrov, G. A. Synthesis, Characterization and Formation Mechanisms of Inorganic Nanomaterials. Thesis, University of California Santa Barbara 2003.

(44) Hiemenz, P. C. Polymer Chemistry: The Basic Concepts 1984, 423-504, New York, NY: Marcel Dekker, Inc.

BIOGRAPHICAL SKETCH

Ryan Oyler was born October 9th, 1978 in the town of Johnstown, PA. He graduated from Pennsylvannia State University in 2001 with a B. S. in Chemistry.

Ryan currently lives in Tallahassee, FL with his his wife and daughter.